metals

MDPI

Article

Effect of Intercritical Annealing and Austempering on the Microstructure and Mechanical Properties of a High Silicon Manganese Steel

Mattia Franceschi [1,*], Luca Pezzato [1], Claudio Gennari [1], Alberto Fabrizi [2], Marina Polyakova [3], Dmitry Konstantinov [3], Katya Brunelli [1] and Manuele Dabalà [1]

1 Department of Industrial Engineering, University of Padua, Via Marzolo 9, 35131 Padova, Italy; luca.pezzato@unipd.it (L.P.); claudio.gennari@unipd.it (C.G.); katya.brunelli@unipd.it (K.B.); manuele.dabala@unipd.it (M.D.)

2 Department of Management and Engineering, University of Padova, Stradella San Nicola 3, 36100 Vicenza, Italy; alberto.fabrizi@unipd.it

3 Department of Mechanical Engineering and Metallurgical Technologies, Nosov Magnitogorsk State Technical University, pr. Lenina, 38, 455000 Magnitogorsk, Russia; m.polyakova-64@mail.ru (M.P.); const_dimon@mail.ru (D.K.)

* Correspondence: mattia.franceschi@studenti.unipd.it; Tel.: +39-0498-275-503

Received: 29 September 2020; Accepted: 27 October 2020; Published: 29 October 2020

Abstract: High Silicon Austempered steels (AHSS) are materials of great interest due to their excellent combination of high strength, ductility, toughness, and limited costs. These steel grades are characterized by a microstructure consisting of ferrite and bainite, accompanied by a high quantity retained austenite (RA). The aim of this study is to analyze the effect of an innovative heat treatment, consisting of intercritical annealing at 780 °C and austempering at 400 °C for 30 minutes, on the microstructure and mechanical properties of a novel high silicon steel (0.43C-3.26Si-2.72Mn wt.%). The microstructure was characterized by optical and electron microscopy and XRD analysis. Hardness and tensile tests were performed. A multiphase ferritic-martensitic microstructure was obtained. A hardness of 426 HV and a tensile strength of 1650 MPa were measured, with an elongation of 4.5%. The results were compared with those ones obtained with annealing and Q&T treatments.

Keywords: austempering; high silicon steel; retained austenite; mechanical properties

1. Introduction

Nowadays, one of the most important objectives of steel producers and researchers in metallurgy is to bring to the market materials with improved properties and performance, high strength-to-weight ratios, and low costs. To achieve these objectives, high-alloyed steels, such aluminum and titanium alloys are not preferred due to the high cost of their raw material; on the contrary, the use of high strength steels (AHSS) is strongly recommended. Great attention is devoted to the study of multiphase steels due to their interesting mechanical characteristics, and both TRIP (TRansformation Induced Plasticity) steels, which belong to the second generation of Advanced High Strength Steels and High Silicon Austempered Steels are considered as more promising.

High silicon austempered steels are attractive grades for their particular combination of mechanical properties and ausfererritic microstructure, which is a mixture of ferrite and high carbon enriched austenite [1,2]. This particular microstructure leads to better mechanical performance, in terms of strength, hardness, and impact toughness in comparison with austempered ductile irons [1].

A silicon weight percentage higher than 1% prevents cementite formation [1–5] and favors austenite carbon enrichment during austempering [6], permitting its retention at room temperature.

According to Zhu et al. [7] silicon also retards static and dynamic recrystallization and retained austenite grain growth, enhancing its stability down to room temperature. Matsumura et al. [4,8] demonstrated that Si slows down bainitic transformation kinetic, widening its stability field.

Furthermore, significant silicon addition raises the critical transformation temperatures (Ac1 and Ac3) in the Fe-C carbon phase diagram [4]. Also. manganese promotes austenite retention, being an austenite stabilizer [4]. Moreover, it prevents pearlite formation, reduces the martensite start temperature (Ms), and delays bainitic transformation. A beneficial effect in term of mechanical properties, due to solid solution strengthening, can also be observed.

Hence, the key to obtain an ausferritic microstructure is to achieve retention and stabilization of a significant amount of retained austenite at room temperature. Retained austenite stability depends on several factors: its carbon content, shape, size, crystallographic orientation, temperature, and the state of the applied stresses [9–12].

A particular heat treatment called austempering, consisting of several steps, should be performed to enable austenite carbon enrichment and consequently its stabilization. During the first step, which is the so called Intercritical Annealing (IA), the material is heated in the dual phase region ($\alpha + \gamma$) between Ac1 and Ac3 [4]. Within this regime a mixture of ferrite and austenite is formed, with different weight fractions depending on the temperature. Austenite dissolves most of the carbon due to ferrite's low carbon solubility but this is not enough to retain austenite at room temperature and further carbon partitioning is required [4]. During the second step, known as the cooling step, additional austenite carbon enrichment takes place due to austenite transformation into ferrite. Most of the carbon is rejected by the newly formed ferrite diffusing into austenite, increasing its stability. The third important part of this treatment is an isothermal soak at temperature for the so called isothermal bainitic transformation (IBT). Part of the remaining volume fraction of austenite transforms in free carbide bainite with low carbon concentration and all the carbon is distributed in the remaining austenite. Once bainitic transformation is completed, the material should be cooled to room temperature retaining a consistent volume fraction of the austenite.

Several works have been devoted to the research of effects of austenitization at intercritical temperatures. According to Yi et al. [13] during IA, austenite nucleates along ferritic grain boundaries (GBs), where carbon is rapidly supplied to austenitic islands. Its growth proceeds rapidly at the beginning and then slows when GBs are saturated with austenite islands. Kang and coworkers demonstrated that the final volume fraction of retained austenite is enhanced by an increase in manganese content [14].

The temperature and holding time of IA have strong influence on the microstructure and mechanical properties of the steels. According to Samajdar et al. [4,15], an increase in annealing temperature reduces the carbon concentration in austenite but increases the martensite start temperature, leading to a decrease in the austenite's stability. This phenomenon was also confirmed by Erişir et al. [16], who also observed austenitic grain growth at higher temperatures. Furthermore, complete recrystallization could be achieved at higher IA temperature, as verified in [4,17]. Emadoddin et al [18] observed that, as the annealing temperature increases, the final volume fraction of residual austenite and its carbon content also increase.

Concerning the soaking time effect on the microstructure during IA, the long dwell time is accompanied by austenite grain growth, which reduces its stability.

Isothermal holding at IBT temperature is the most important step of the heat treatment [4]. If the soaking is performed at a temperature close and/or corresponding to the nose of the bainitic transformation, the time to complete the bainitic transformation is reduced. Moreover, the longer the holding time, higher the bainite volume fraction and the carbon partitioned in austenite, and this produces an increase in the austenite's stability.

Another relevant heat treatment consists in Quenching and Partitioning (Q&P). The treatment differs substantially from Quenching and Tempering (Q&T), which is a common treatment in industrial applications [19,20]. During Q&P, once steel is austenitized, it is quenched at a temperature between martensite start temperature (Ms) and Mf (martensite finish temperature) and then soaked at the

so-called partition temperature (PT). At PT carbon diffuses from martensite to retained austenite favoring its retention at room temperature and enhancing strength and ductility [21].

Moreover martensite, formed after quenching, speeds up the kinetic of bainitic transformation and the process of austenite stabilization [22,23].

Oliveira et al [21], analyzing the behavior of a MnSi steel after austempering and Q&P, observed that in the first case a microstructure consisting in a mixture of plate and granular bainite, martensite, and retained austenite is present. After Q&P a martensite matrix with bainitic islands and austenite films/blocks is instead formed.

Novelty of the Work

In this paper, a new dual phase high silicon steel with a novel composition was investigated. The effect of intercritical annealing and austempering on microstructure and mechanical behavior was studied The samples were characterized by optical microscopy (OM, LEICA DMRE, Leica Microsystems S.r.l., Milan, Italy), scanning electron microscopy (SEM, LEICA™ Cambridge Stereoscan LEO 440, Leica Microsystems S.r.l., Milan, Italy, EBSD, AMETEK BV, Tilburg, The Netherlands), transmission electron microscopy (TEM, JEOL JEM 200CX, Jeol Ltd, Tokyo, Japan), X-ray diffraction (XRD, Bruker D8 Advance, Karlsruhe, German) techniques, and mechanical tests. The results were compared with those obtained after annealing and Q&T treatments.

2. Materials and Methods

The material used in this study was a high silicon manganese steel, produced by Magnitogorsk Nosov State Technical University of Magnitogorsk (Russia). The chemical composition is presented in Table 1.

Table 1. Chemical composition of the investigated alloy (wt.%).

C	Si	Mn	P	S	Cr	Ni	Cu	Mo	Ti	V	Al
0.43	3.26	2.72	0.010	0.0082	0.043	0.074	0.060	0.022	0.0010	0.0051	0.105

The steel was prepared melting high purity raw material in an induction furnace. Liquid metal was cast, and the produced ingots were forged, and water cooled to room temperature

2.1. Heat Treatments

Heat treatment setup was composed by a Carbolite tubular electrical furnace and Nabetherm 3000 muffle electrical furnace. Tubular furnace was used for austenitization during quenching and for tempering the samples. It was also used for the intercritical annealing step. The other furnace was employed for austempering treatment. An air-cooling system was realized for the cooling step from the biphasic region to the Isothermal Bainitic transformation temperature. The final cooling to room temperature, from the IBT temperature, was performed in water. The samples' temperatures were recorded during the heat treatments with a K-thermocouple.

Heat treatments were designed using JmatPro software. A theoretical phase diagram was built to study the biphasic austenite-ferrite region, to evaluate the volume fraction of the two microstructural constituents and to determine austenite composition as a function of temperature (Figure 1). The obtained information permitted us to choose the temperatures to perform the IA step, highlighted by the red line in Figure 1b. Theoretical CCT and TTT curves (Figure 2) were built to define required cooling rates in the transition between annealing and the second austempering phase. This operation was necessary to avoid ferrite and perlite precipitation during treating cycles. Finally, holding times in the bainitic region were set thanks to the relative start and end transformation curves.

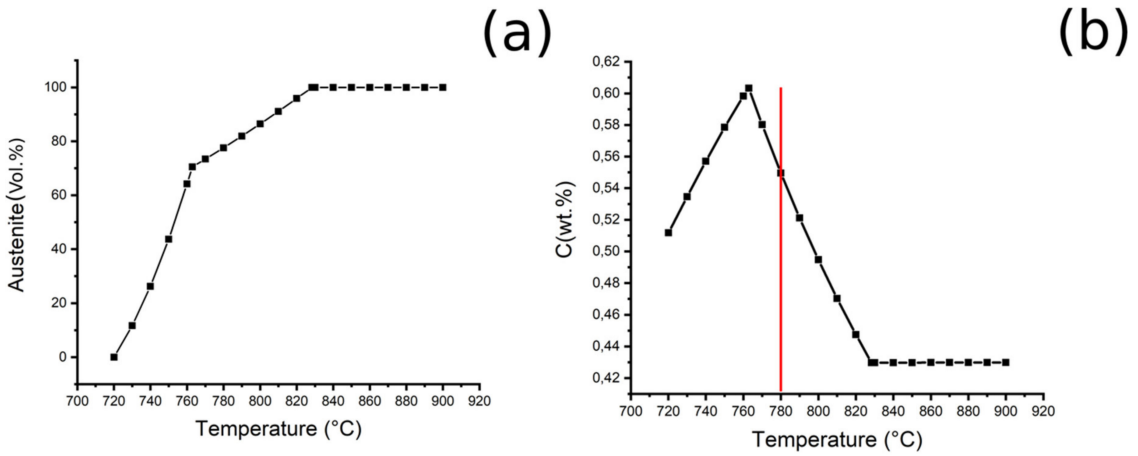

Figure 1. Volume percentage of austenite (**a**) and carbon content (**b**) as a function of temperature during austenitization. The red line in (**b**) indicates intercritical annealing condition.

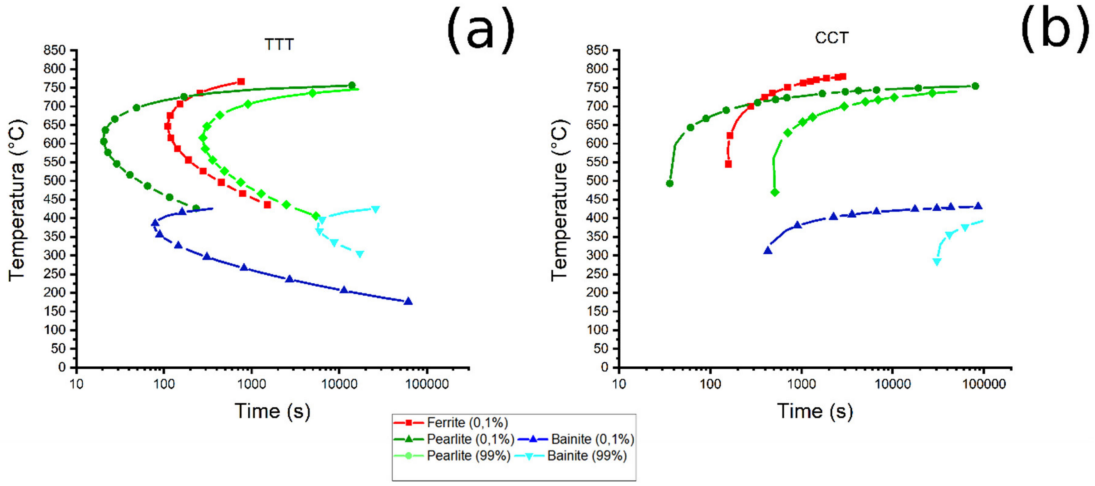

Figure 2. (**a**) TTT, (**b**) CCT curves calculated with JMat Pro software for heat treatment design.

We decided to perform the intercritical annealing with the parameters reported in Table 2.

Table 2. Intercritical annealing parameters.

A_{c1} (°C)	A_{c3} (°C)	Interctritical Annealing Temperature (°C)	Ferrite (wt.%)	Austenite (wt.%)	C_γ (wt.%)
~763	~839	~780	~23	~76	0.55

For each treatment described below, three samples were prepared.
To summarize, the subsequent heat treatments were performed:

i. *Annealing*: heating at 870 °C at 1 °C/s, 10 min holding time and furnace cooling (0.15 °C/s).
ii. *Quenching and tempering (Q&T)*: heating at 900 °C at 1 °C/s, 15 min dwell time, and water quenching (cooling rate: 40 °C/s); tempering at 600°C for 30 min and air cooling (5 °C/s) (Figure 3a).
iii. *Intercritical Annealing and Austempering (IA&A)*: Pre-quenching treatment from 870 °C (15 min) and water cooling. Heating at 780 °C for 30 min at 0.8 °C/s, air cooling at 10 °C/s to 400 °C and holding for 30 min followed by water cooling to room temperature at 40 °C/s (Figure 3b).

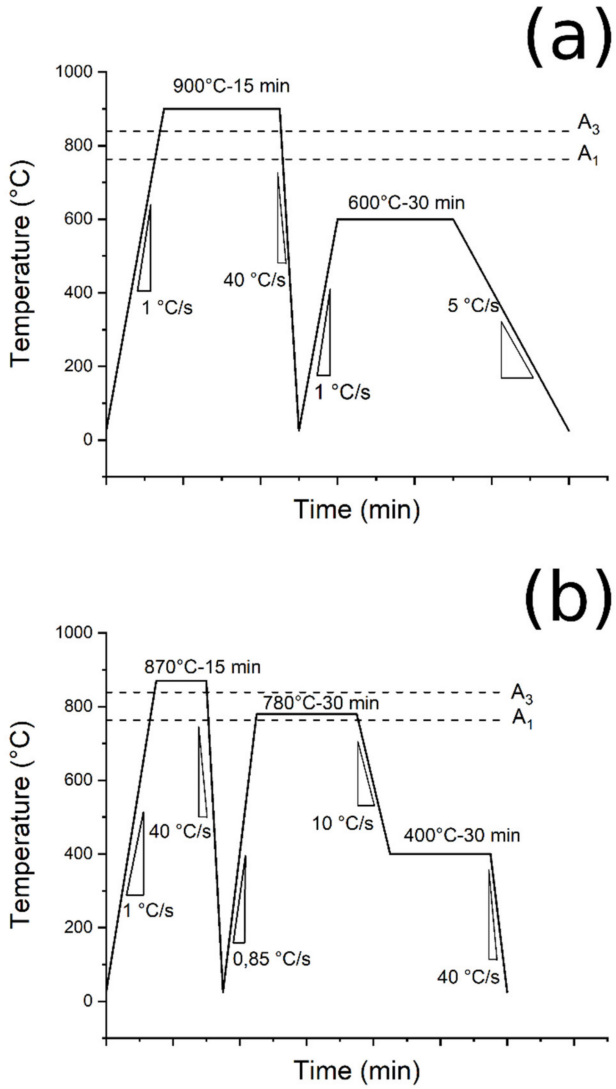

Figure 3. Heat treatment processing scheduled for the high silicon steel: (**a**) Quenching and Partitioning (Q&P), (**b**) Austempering.

The heat treatments were performed starting from a martensitic microstructure, because martensite allows for the faster recrystallization processes of ferrite during intercritical annealing and higher performance after the treatment, according to other works [4,24,25]. Furthermore, Kim et al. [4,25] demonstrated that fine microstructure, resulting from a rapid cooling, favors austenite formation and its carbon enrichment when material is re-heated.

2.2. Microstructural Study

The microstructure of the samples was analyzed along the cross section of the specimens. To perform the analysis an optical microscope, LEICA DMRE (Leica Microsystems S.r.l., Milan, Italy), and a scanning electron microscopy (SEM) LEICA™ Cambridge Stereoscan LEO 440 (Leica Microsystems S.r.l., Milan, Italy) were used. The preparation of the samples was carried out following the standard technique. The specimens were cut with SiC discs lubricated with a mixture of water and oil, mounted in phenolic resin, grinded with SiC papers (320, 500, 800, 1200 grit), polished with clothes and 6 µm and 1 µm polycrystalline diamond suspensions. EBSD analysis occurred after the samples were further polished with 200 nm and 40 nm silica colloidal particles suspension. In order to reveal the microstructure of the samples they were etched with Nital 2.

Phase identification and phase quantification were carried out through X-ray diffraction with a Bruker D8 Advance (XRD, Bruker D8 Advance, Karlsruhe, German), operating at 40 kV and 40 mA and a Cu radiation tube (Kβ radiation was filtered by mean of nickel filter on the tube side). The investigated angular range was between 40° and 105°, steps scan of 0.025° and counting time of 3 s. The obtained patterns were analyzed using High Score Plus software in order to identify the constituent phases. Volume fraction calculation of the phases was performed through Rietveld analysis on the same software.

Electron Backscattered diffraction (EBSD) analysis was performed after the heat treatments in order to study in detail the obtained microstructure. In particular, the identification and quantification of the phases were carried out. Moreover, phase distribution, orientation, and the presence of textures were investigated. For EBSD investigations, we used a FEI QUANTA 205 FEG SEM (Thermo Fisher Scientific, Hillsboro, OR, USA), equipped with AMETEK EBSD (AMETEK BV, Tilburg, The Netherlands) system and OIM Analysis™, operating at 20 kV. The analyses were performed with the following parameters: Scan step: 200 nm, area: ~150 × 200 μm^2; confidence Index >5% and Scan step: 100 nm; area: ~35 × 40 μm^2, confidence Index >5%.

Transmission electron microscopy (TEM) was also performed to complete the characterization of RA on the samples using a JEOL JEM 200CX (Jeol Ltd, Tokyo, Japan) operating at 160 kV. The preparation of the thin foils was realized by mechanical grinding until thickness of 70 μm, followed by mechanical punching to obtain 3 mm diameter specimens. The final polishing and etching were performed electrochemically using a twin-jet polisher STRUERS TENUPOL-3 (Struers S.A.S., Milan, Italy), with 95% acetic acid (CH_3COOH) and 5% perchloric acid ($HClO_4$) solution, at 45 V and room temperature [26,27].

2.3. Mechanical Tests

Vickers micro-hardness, with a Leitz™ DURIMET (Leica Microsystem S.r.l., Milan, Italy) hardness tester, were conducted on each sample performing three indentations, with a 300 g load.

The treated samples were also subjected to tensile tests according to ASTM A370 $\varepsilon^{19'1}$. The tests were carried out on dog-bone samples, at strain rate of 5×10^{-3} s^{-1} with a MTS tensile test machine (MTS System Corporation, Eden Prairie, MN, USA), using a maximum force of 50 kN. The displacement was measured through the crosshead movement and the force by the machine load cell.

3. Results

3.1. Microstructure

The microstructure of the as-received material is shown in Figure 4a–c. The as-received structure shows a predominant martensitic matrix with some allotriomorphic ferritic colonies (F_A) formed at the prior austenitic grain boundaries during quenching. From the SEM micrograph (Figure 4b,c) it can be further observed the presence of idiomorphic ferrite (F_I), nucleated inside the original austenite grains (GB), present before the quenching.

Figure 5a–c reports the evolution of the microstructure caused by the annealing treatment at 870 °C for 10 min. From OM and the SEM micrograph (Figure 5a,b) it is possible to observe the presence of pearlitic islands (P). In the red box, shown in Figure 5c at higher magnification, eutectoidic islands with different lamellae orientation, surrounded by ferritic (F) grains, can be distinguished. This is the typical microstructure of a medium carbon steel after annealing treatment [28].

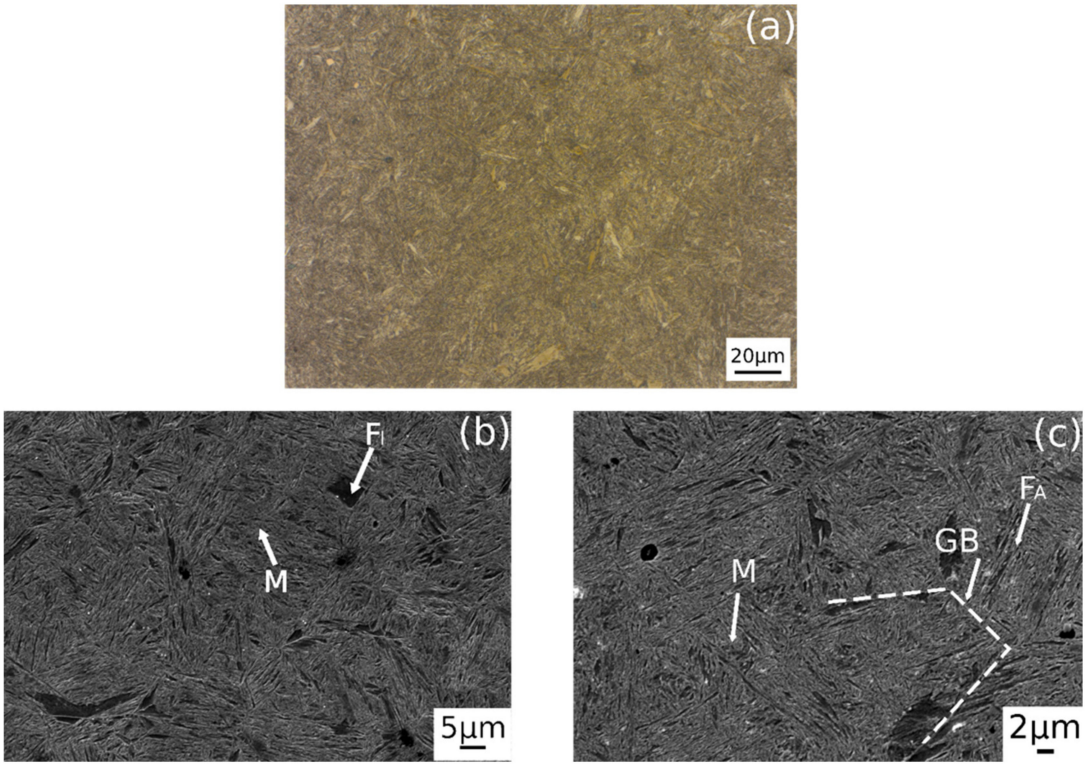

Figure 4. Optical (**a**) and SEM (**b**,**c**) micrographs showing the microstructure of the material in as-received state.

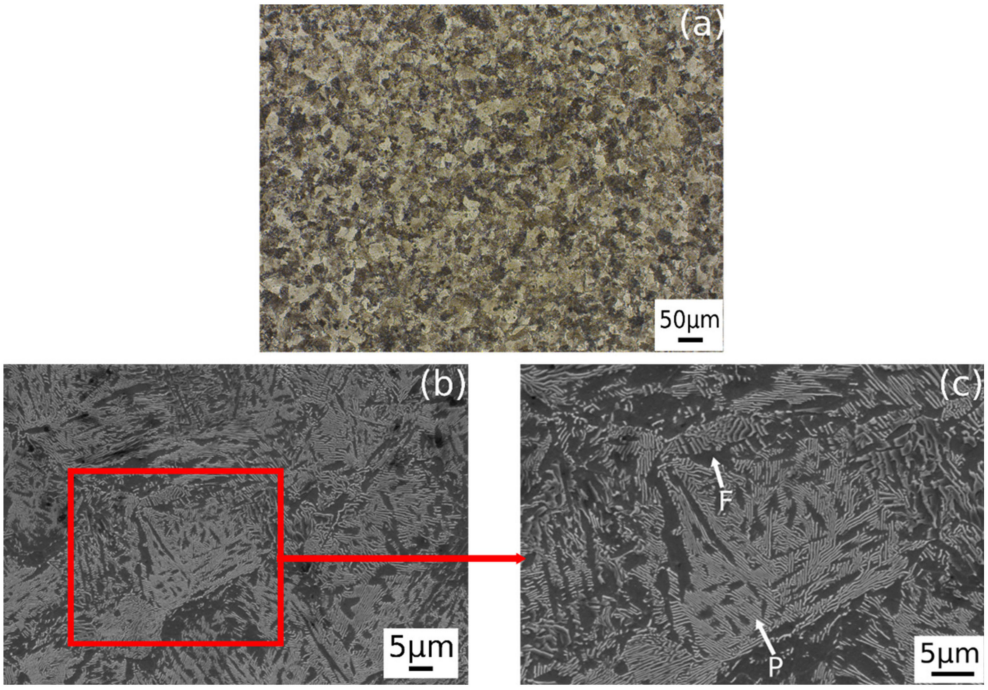

Figure 5. Optical (**a**) and SEM (**b**,**c**) micrographs showing the microstructure after annealing at 870 °C.

Figure 6 refers to the microstructure of the material after water quenching, before tempering. As expected, a complete martensitic microstructure (M) was obtained. SEM images (Figure 6b,c) reveal

the presence of allotriomorphic ferrite, indicated in the image with F_A at the prior austenite grain boundaries (GB) [29,30]. In Figure 7c idiomorphic ferrite (F_I) at the center of the grain is shown.

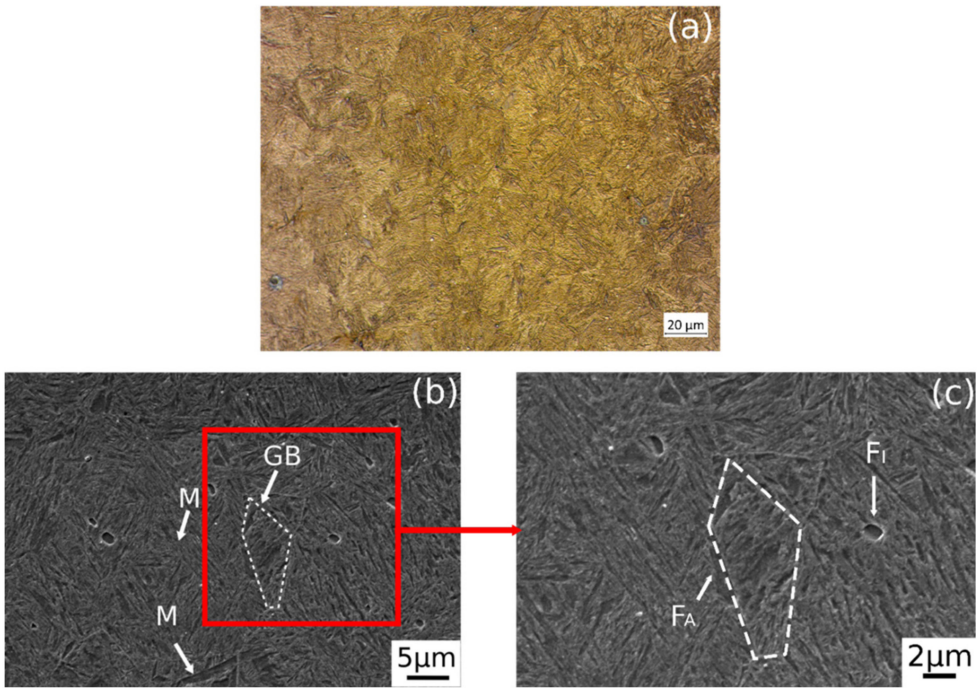

Figure 6. Optical (**a**) and SEM (**b**,**c**) micrographs after water quenching from 900°C (15 min holding).

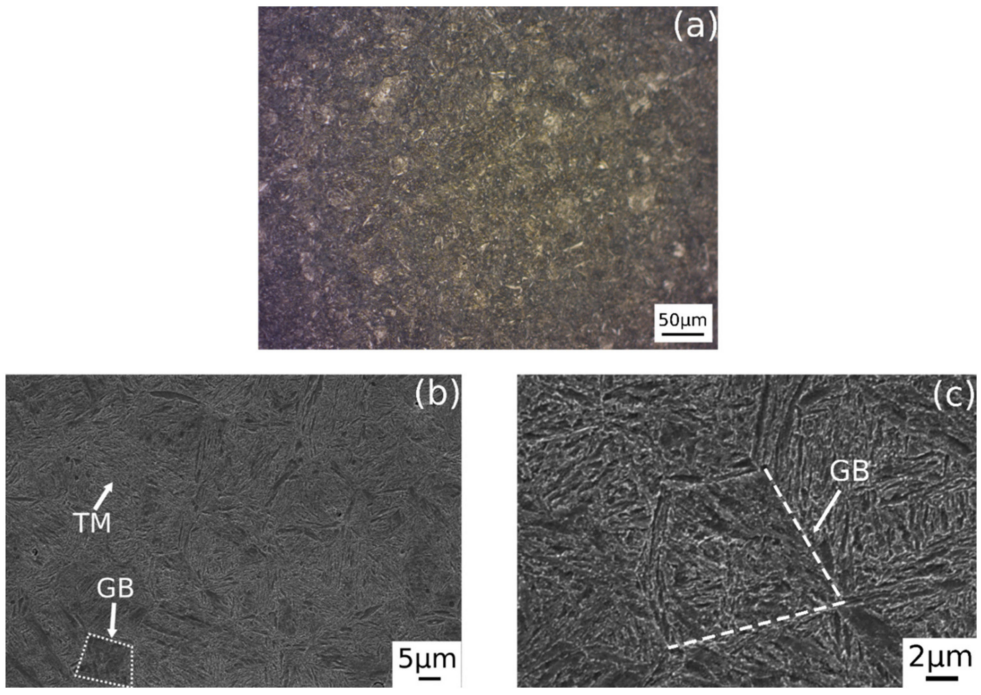

Figure 7. Microstructure of material after tempering at 600 °C and air cooled. (**a**) Optical micrograph, (**b**) and (**c**) SEM micrograph.

After tempering treatment, the material shows a microstructure consisting of tempered martensite (TM), as reported in Figure 7. SEM analysis (Figure 7b,c) allows us observe the presence of tempered martensite and trace of prior austenite grain boundary (GB).

After Quenching, Intercritical Annealing, and Austempering treatments, the samples show a different microstructure compared to that of the previous ones. It is possible to observe (Figure 8a,b) a dual phase microstructure, characterized by the presence of ferrite surrounded by a martensitic matrix and retained austenite. Ferrite is formed during the intercritical annealing at 780 °C. The ferrite presents in microstructure, visible in Figure 8, is a combination of different types and morphologies. A certain volume fraction of ferrite is formed during the intercritical annealing in the biphasic region. It is also possible to observe allotriomorphic and idiomorphic ferrite, as result of the partial transformation of austenite during the first cooling phase. The formation of these kinds of ferrite contributes strongly to the carbon enrichment of austenite. The low carbon solubility of ferrite forces carbon partitioning in austenite, increasing its stability and the possibility to retain it at room temperature. Martensite derives from austenite formed during heating in biphasic regime; austenite partially transforms into ferrite during the first heating step and into martensite during the last cooling phase. Bainite is not present during the austempering phase of the treatment and it is not visible in the microstructure, even if expected from the cooling transformation curve. This phenomenon could be related to the evolution of the curves and transformation temperatures caused by carbon partitioning during the heat treatment steps. It can be supposed that carbon partitioning leads to a decrease of Bs.

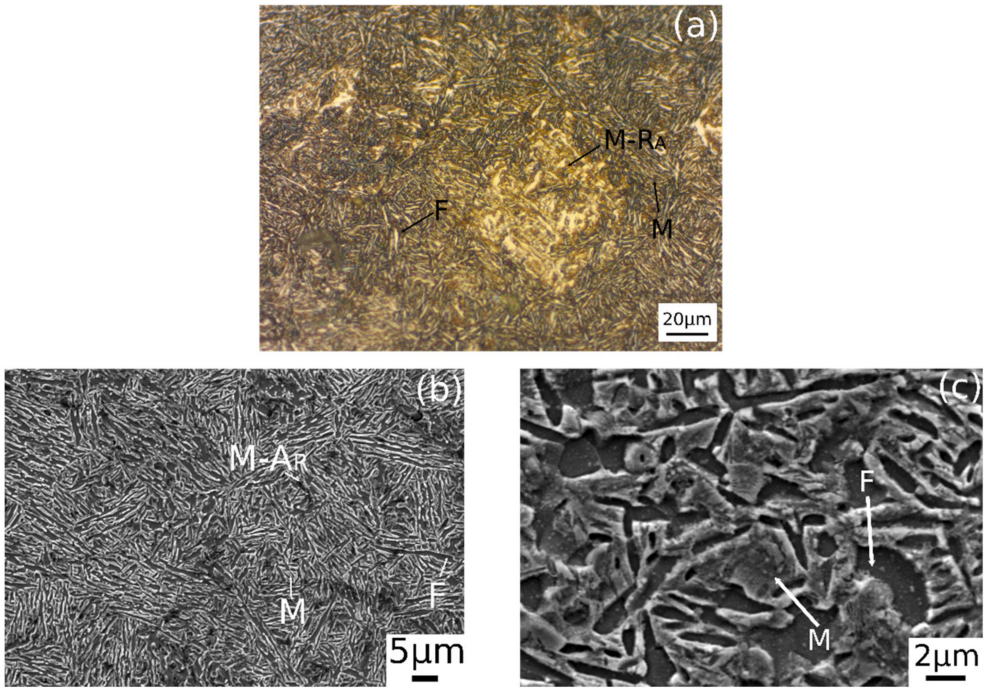

Figure 8. Microstructure of material after austempering. (**a**) Optical micrograph, (**b**) and (**c**) SEM micrograph.

FEG-SEM micrograph (Figure 9), taken in backscattered electron mode, allows us to see in detail the microstructure of the specimen subjected to austempering treatment. In the red box Figure 9b, it is clearly visible lath martensite in light grey and ferrite in black. This type of martensite morphology was confirmed in a research work by Ahmad and colleagues, which demonstrated that with intercritical annealing a lath morphology is acquired [31].

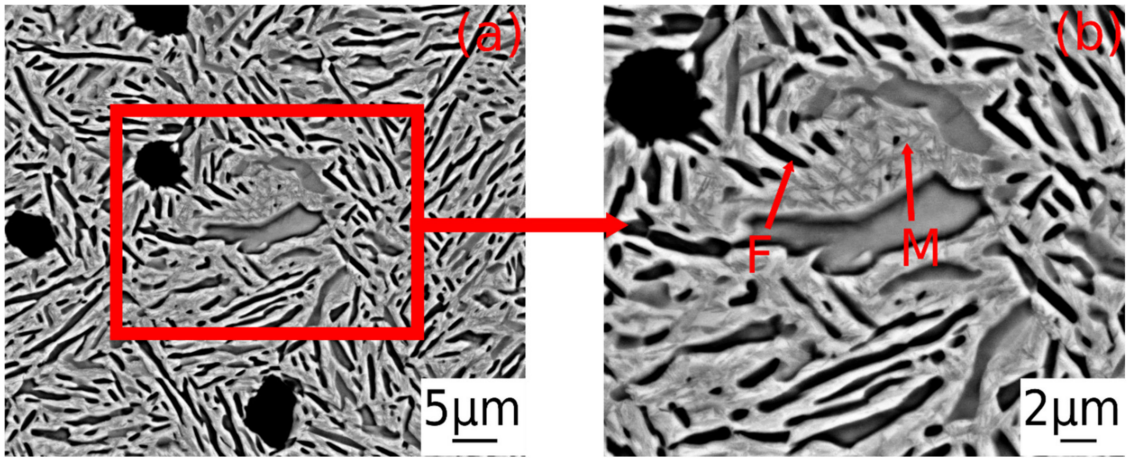

Figure 9. (**a**) Backscattered electrons FEG-SEM image of specimen subjected to Austempering (**b**) lath martensite detail.

3.2. X-ray Diffraction

One of the main goals of this thermal cycle is to achieve a multiphase material with a sufficiently high carbon content in the retained austenite which promote its retention at room temperature and leads a significant volume fraction of RA.

Figure 10 reports the X-ray diffraction patterns of the specimens subjected to annealing, Q&P, and Austempering heat treatment. X-ray pattern of annealed sample (Figure 10a) shows BCC iron peaks in the investigated angle range. Moreover, as 2θ increases it is possible to resolve Kα1 and Kα2 line peaks (indicated with the arrows). This could be related with the presence of coarse grains, which allows a better peak definition and high pattern resolution.

A slight difference in the peak position in the X-ray patterns can be observed, which could be attributed to the different dimension of the cell, caused by the different heating cycles.

Asymmetrical broadening of ferrite diffraction peaks towards low 2θ angles can be observed in the austempered samples (Figure 10b). Those peaks are related to the presence of tetragonal martensite. The presence of a displacement between ferrite and martensite peaks is due to the high carbon content of martensite and the strong distortion of the cell [32].

The presence of martensite in samples can be related to room temperature cooling that causes austenite transformation. High carbon austenite, which is not transformed in bainite during austempering, transforms in martensite when cooled down.

The X-ray diffraction technique allowed us to confirm the presence of retained austenite in the austempered samples, with a volume fraction similar to the one found in several TRIP steels and austempered high silicon steels [4]. The results of the phase quantification, reported in Table 3, demonstrate that the treatment cycle favors the process of carbon partitioning, allowing austenite retention at room temperature.

Table 3. Rietveld analysis results for phase quantification for the austempered sample.

Retained Austenite (%)	Martensite (%)	Ferrite (%)
14.9	40.5	44.6

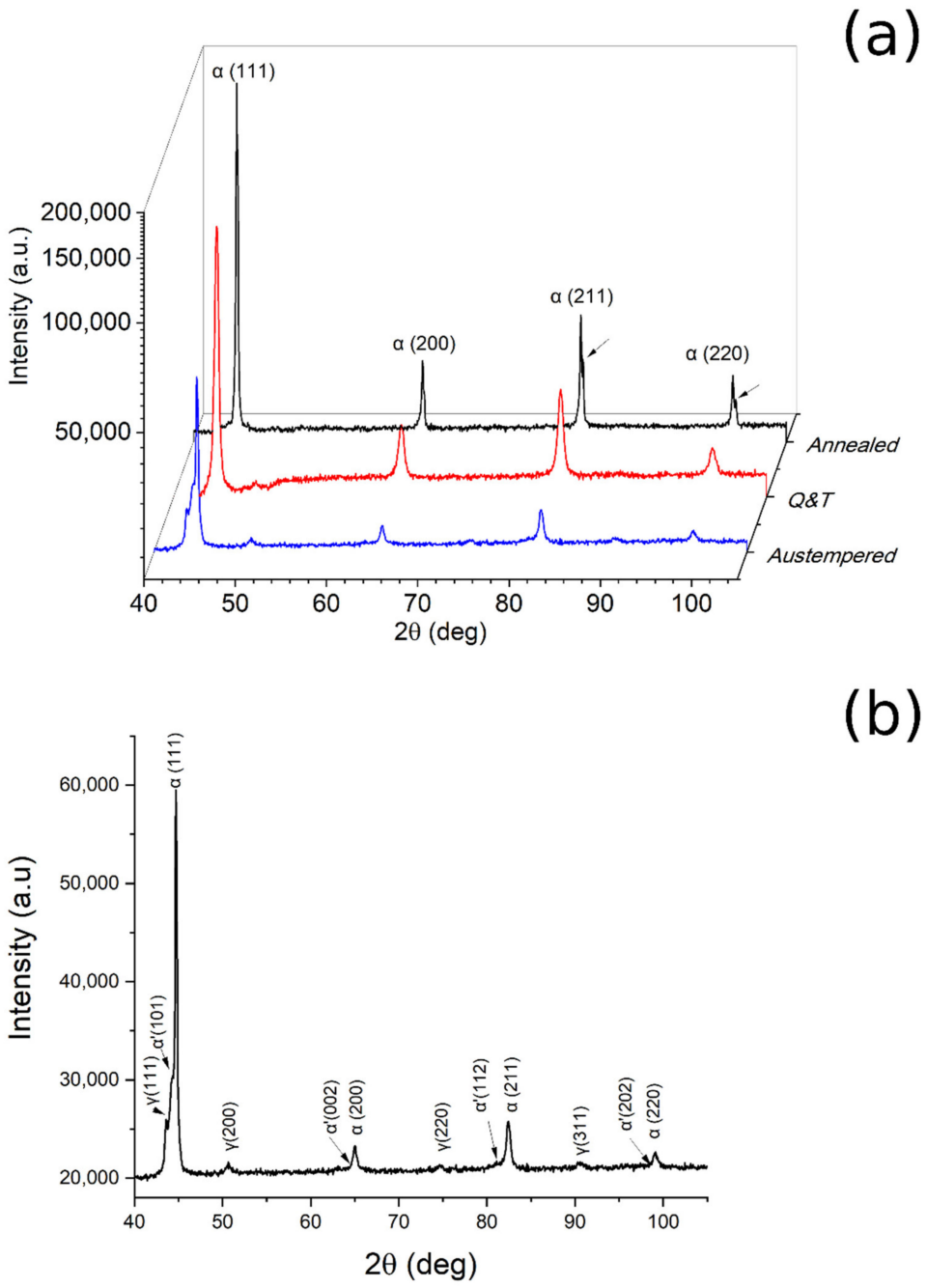

Figure 10. X-ray diffraction pattern of high silicon steel after each heat treatment (**a**), X-ray pattern of austempered steel in detail (**b**).

3.3. Electron BackScattered Diffraction

In order to better analyze the microstructural features of the austempered samples, EBSD analysis was performed. The main goal of the investigation was to understand distribution retained austenite, and its morphology and size.

No preferential orientation was observed in the material subjected to the austempering treatment (Figure 11). The absence of texture and preferred grain orientation can be explained considering that: a) the material was not subjected to deformation or forming process during heat treatment, b) a pretreatment, which produces recrystallization, was performed.

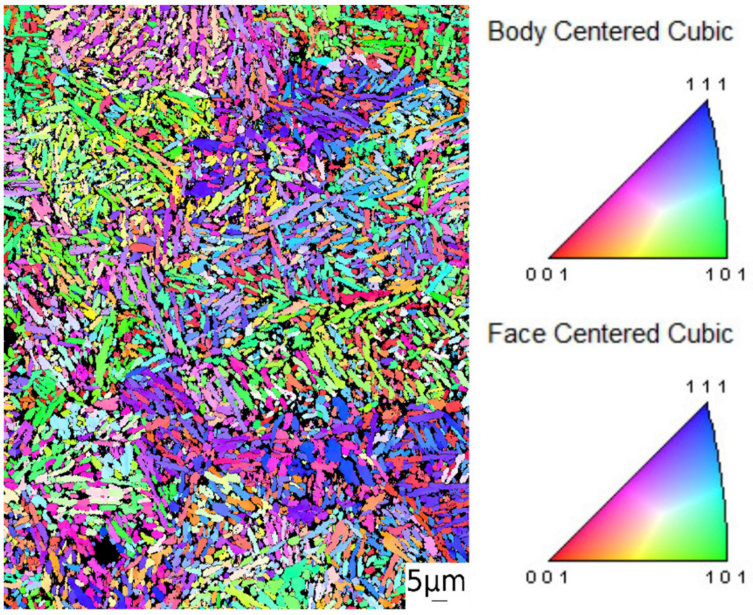

Figure 11. Electron Backscattered diffraction (EBSD) micrograph and related inverse pole figure of the austempered sample.

Figure 12 shows the detailed EBSD analysis on smaller sample areas. It can be noted also in this case that each phase has randomly oriented grains (Figure 12a). In Figure 12b, a phase distribution map is shown: red zones represent FCC iron, green ones refer to tetragonal martensite and retained austenite (FCC iron) is colored in yellow. A matrix of ferrite can be distinguished, with uniformly distributed austenitic and martensitic islands. Austenite is located at ferrites grain boundaries close to the martensitic islands, with a grain size of 1–5 µm. Such dimension of the FCC iron refer to high stable austenite with high carbon content. These islands should exhibit a strain induced martensitic transformation during plastic deformation at high strains [4,9,10,33–39].

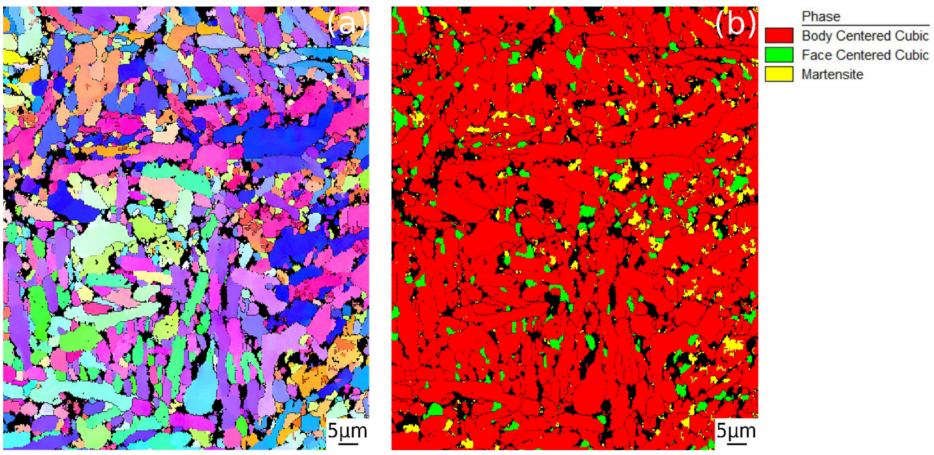

Figure 12. Detailed inverse pole (**a**) figure and phase identification of the material subjected to austempering treatment (**b**).

3.4. Transmission Electron Microscopy

A further microstructural investigation was carried out by TEM on the austempered samples (Figure 13a,b) in order to deeply analyze the morphology of the martensitic–austenitic regions formed during the heat treatment and shown with the other techniques.

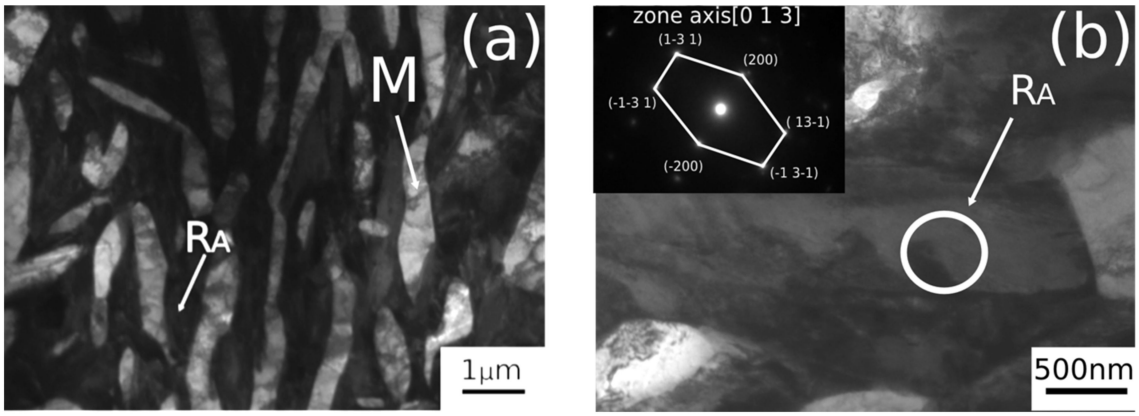

Figure 13. TEM micrographs (**a**) and (**b**) and electron diffraction patterns.

Figure 13a shows the presence of martensitic zones (light grey islands) and films of retained austenite (black islands). A detail of a retained austenite film between martensitic region is shown in Figure 13b. SAED was performed in the correspondence of the white circle zone, and the resulting diffraction pattern, indexed according to [40], confirm the presence of austenite. Therefore, it is possible to state that the treatment allows the austenite retention, due to the carbon partitioning.

EBSD and TEM analysis show that retained austenite has two morphologies: films between martensitic islands and blocks. The obtained retained austenite is characterized by different carbon content and different stability, in particular RA located near the martensitic islands is richer in carbon and more stable, according to [41]. Blocky austenite, which is poor in carbon, transforms earlier than lath austenite during the deforming process, as evidenced by [9].

3.5. Mechanical Properties

3.5.1. Microhardness Test

Microhardness results are reported in Table 4. It is possible to observe that the material, when annealed, has lower hardness compared to the samples subjected to the other treatments. Moreover, material subjected to austempering treatment has higher hardness than the sample treated by Q&T. The lower hardness of the Q&T sample could be explained considering the effect of the tempering treatment on martensite. The subsequent heating of martensite, below austenitization temperature, favors stress release, carbon diffusion, and carbide precipitation.

Table 4. Microhardness on material before tensile test.

Treatment	Average ($HV_{0.3}$)	St. Deviation
Annealed	316	22
Q&T	364	29
Austempering treatment	426	19

3.5.2. Tensile Tests

Mechanical properties were evaluated in terms of yield strength (YS), ultimate tensile strength (UTS), and fracture strain. The specimens, after annealing treatment and Q&P, showed the highest uniform elongation (Figure 14 and Table 5), while after austempering treatment the sample exhibited poor elongation, without evident yielding and plastic deformation. In detail, in the austempered sample, a fracture strain of approximately 4.5% and UTS of 1650 MPa were recorded. The brittle nature of the material could be explained considering the amount of martensite and its high dislocation density which limits further plastic deformation and the low strength of the martensite-ferrite cohesion.

A similar behavior was observed by Ahmad and colleagues [31]. The presence of a slight plastic deformation can be attributed to the presence of a considerable amount of ferrite.

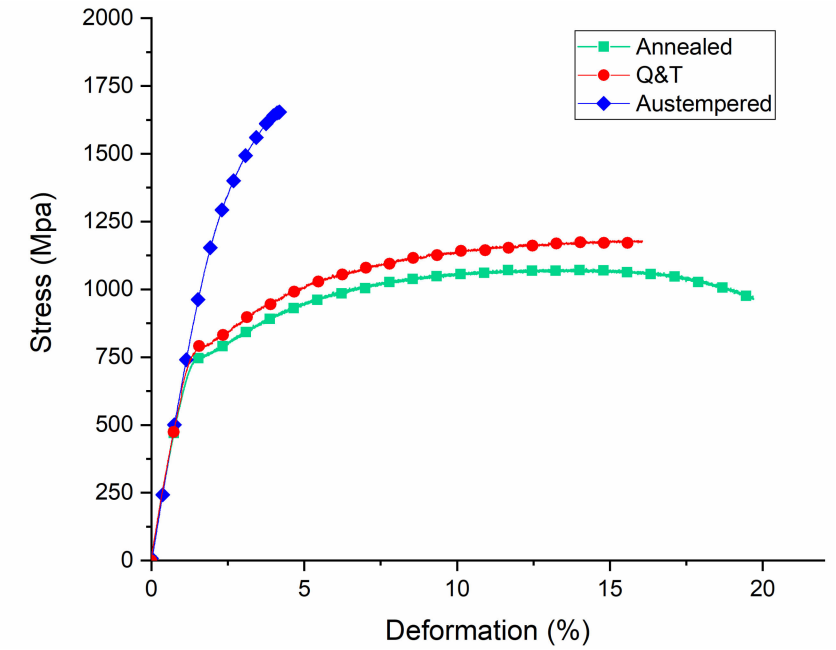

Figure 14. Engineering stress-strain curves. Blue curve with blue circle is related to austempered samples, red curve with diamonds referred to the Q&P treatment and green curve with squares representing the annealed samples.

Table 5. Results of tensile tests.

Material	Yield Strength (MPa)	Tensile Strength (MPa)	Fracture Strain (%)
Annealed	730	1130 ± 5	20 ± 2
Q&T	760	1200 ± 5	16.5 ± 2
Austempering treatment	1250	1650 ± 5	4.5 ± 0.5

The fracture surface of specimens after annealing (Figure 15) shows the typical features of a ductile fracture, confirming the mechanical behavior evidenced in the stress-strain curves. It also is possible to observe in Figure 15b the fracture surfaces of pearlitic grains [42].

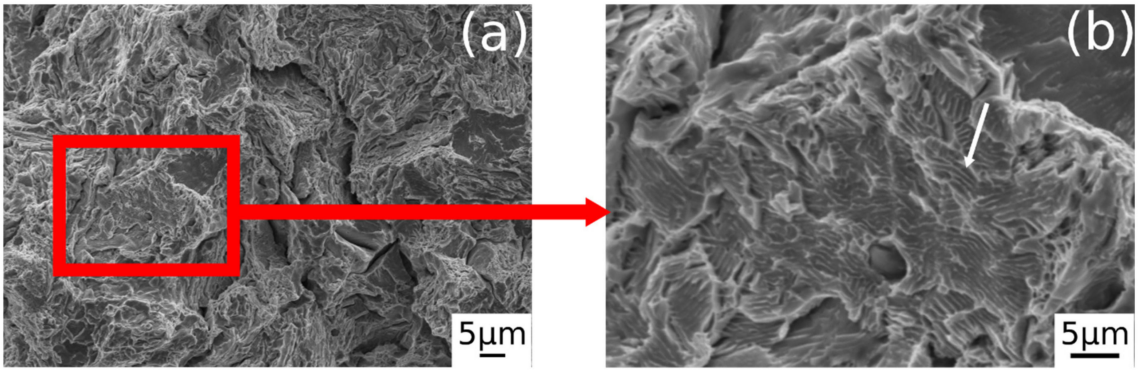

Figure 15. (**a**) SEM fractography of the sample in annealed condition (**b**) detail of a pearlitic fractured grain. White arrow in (**b**) indicates fracture surface of a pearlitic grain.

Figure 16 shows fracture surfaces of the material after Q&P, also in this case the material exhibits ductile fracture and are recognizable dimples indicated in Figure 16b with white arrows.

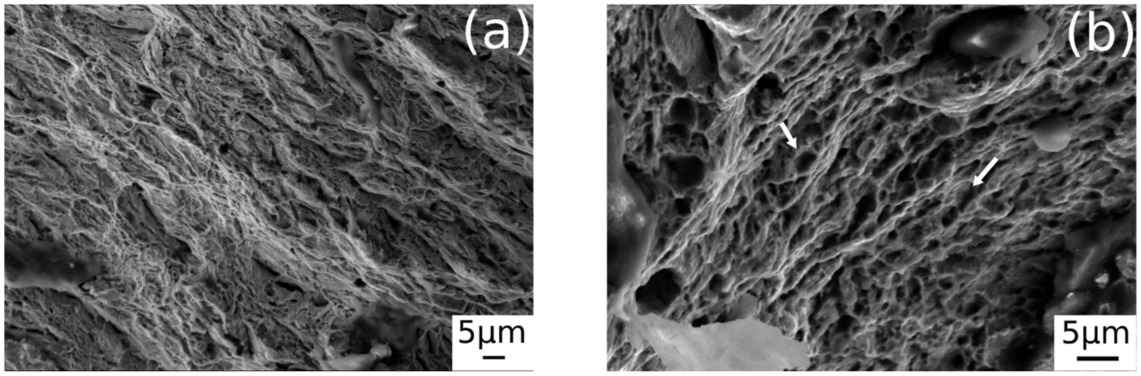

Figure 16. (**a**) SEM fractography of the sample in annealed condition (**b**) fractography showing dimples (indicated by white arrrows).

Brittle failure could be observed in the case of austempered specimen (Figure 17), with the development of cleavage facets [31], highlighted in the figure by circles.

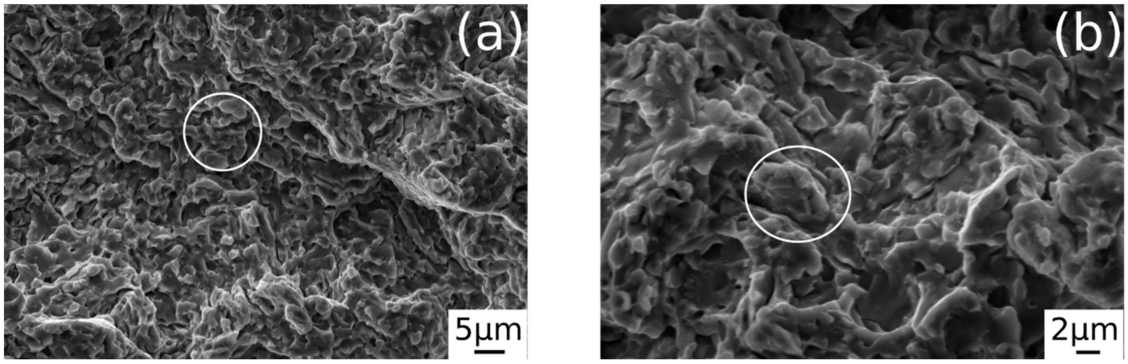

Figure 17. SEM fractography showing the fracture surface (in white cyrcles) revealing cleavage facets in Austempered samples (**a**) and (**b**).

4. Discussion

4.1. Austempering Treatment

The austempering treatment was performed in correspondence with the bainitic region nose in order to minimize the soaking time due to the fast kinetics (Figure 1). In fact, the time required to complete the transformation is the shortest and the transformation is also anticipated, reducing the overall time of the heat treatment [1].

4.2. Microstructure and Mechanical Properties

The annealing treatment, as shown in Figure 5, produced a microstructure consisting of pearlite and ferrite, as expected. The material is characterized by an equiaxed grain structure with eutectoidic islands randomly oriented, while quenching and tempering allowed us to obtain tempered martensite (Figure 7). The microstructure obtained after these two treatments agree with the ones reported in literature.

The austempering treatment produced a completely different microstructure; in fact, the observation carried out on the samples with optical and scanning electron microscopes (Figure 8)

revealed the presence of a multiphase microstructure. This microstructure consists of ferrite, martensite, and retained austenite.

During soaking at IBT temperatures a significant fraction of austenite stabilized due to the carbon in FCC iron. After the heat treatment, retained austenite showed two morphologies: i) films between martensite laths, and ii) blocks according to [9,33,35–38,43,44]. The authors also observed that the austenite carbon content was not homogeneous, in particular, it was higher in the first type of retained austenite compared to the blocky austenite.

No upper or lower bainite was present in the microstructure, as expected. As a matter of fact, carbon partitioning, which takes place during the treating cycles, especially during annealing and the first cooling phase, may modify bainite start temperature (Bs). In detail, the increase in the carbon content in austenite can reduce Bs, as predicted in some models, as those reported by Lee [45]

Concerning the mechanical properties, the hardness values agreed with the microstructure present in the samples. The austempering treatment produced and increased hardness, due to the high volume fraction of un-tempered martensite, and the results are in accordance with the behavior reported in literature [46]. The Q&T sample was characterized by lower hardness, due to martensite tempering which led to martensite transformation and internal stress reduction.

Hardness and microstructural constituents can also explain tensile test results. The samples subjected to annealing treatment exhibited coarser microstructure and lower hardness and tensile strength compared to the other samples but were characterized by the highest ductility.

Considering the austempering treatment, the samples with the highest hardness values and the highest tensile strength, with a predominantly brittle behavior, were obtained. The brittle phenomenon was also confirmed by the fractographs, in which were not visible the features typical of a ductile fracture. This behavior is certainly determined by the microstructure, which mainly consisted of martensite, while the just mentioned plastic deformation was attributed to the ferrite volume fraction.

5. Conclusions

- A novel high silicon steel with multiphase microstructure composed by ferrite, tetragonal martensite, and retained austenite was developed. Austempering treatment allowed us to stabilize a consistent volume fraction of retained austenite equal to 14.9%.
- The complete XRD, EBSD, and TEM analysis revealed that RA is present in two morphologies: as film between martensite islands and in form of blocks.
- The sample subjected to austempering exhibits the higher values of Vickers microhardness while Q&T and annealed samples are characterized by lower values.
- Austempering treatment enhances material tensile strength (1650 MPa), in comparison with annealing and Q&T, which are characterized by lower tensile tests, 1130 and 1200 MPa respectively. However, the high amount of martensite, is responsible of low fracture strain (4.5%) and ductility, which is confirmed by the brittle fracture surface.

Author Contributions: Conceptualization, M.D., M.P., K.B.; methodology, C.G., L.P.; software, D.K., M.F.; validation, D.K., C.G.; formal analysis, M.F., D.K.; investigation, M.F., A.F., L.P., C.G., L.P.; resources, D.M., K.B., M.P.; data curation, M.F., C.G.; writing—original draft preparation, M.F., L.P., C.G.; writing—review and editing, L.P., C.G.; visualization, M.F., C.G.; supervision, K.B., M.P., M.D.; project administration, M.D., M.P.; funding acquisition, M.D., M.P. All authors have read and agreed to the published version of the manuscript.

Funding: The authors want to thank FONDAZIONE CARIPARO for the financial support with the visiting program TIP-STEP.

Acknowledgments: The authors want to thank Marco Breda from Unilab Laboratori Industriali S.r.l., for the tensile tests.

Conflicts of Interest: The authors declare no conflict of interest.

References

1. Mandal, D.; Ghosh, M.; Pal, J.; De, P.K.; Ghosh Chowdhury, S.; Das, S.K.; Das, G.; Ghosh, S. Effect of austempering treatment on microstructure and mechanical properties of high-Si steel. *J. Mater. Sci.* **2009**, *44*, 1069–1075. [CrossRef]
2. Putatunda, S.K.; Singar, A.V.; Tackett, R.; Lawes, G. Development of a high strength high toughness ausferritic steel. *Mater. Sci. Eng. A* **2009**, *513–514*, 329–339. [CrossRef]
3. Vuorinen, E.; Chen, X. In-situ high temperature X-ray studies on bainitic transformation of austempered silicon alloyed steels. *Mater. Sci. Forum* **2010**, *638–642*, 3086–3092. [CrossRef]
4. Fonstein, N. *Advanced High Strength Sheet Steels: Physical Metallurgy, Design, Processing, and Properties*; Springer: Cham, Switzerland, 2015; ISBN 9783319191652. pp. 1–396.
5. Edmonds, D.V.; Cochrane, R.C. Structure-property relationships in bainitic steels. *Metall. Trans. A* **1990**, *21*, 1527–1540. [CrossRef]
6. Zhu, L.-J.; Di, W.U.; Zhao, X.-M. Effect of Silicon Content on Thermodynamics of Austenite Decomposition in C-Si-Mn TRIP Steels. *J. Iron Steel Res. Int.* **2006**, *13*, 57–60. [CrossRef]
7. Zhu, L.J.; Wu, D.; Zhao, X.M. Effect of silicon addition on recrystallization and phase transformation behavior of high-strength hot-rolled trip steel. *Acta Metall. Sin. Engl. Lett.* **2008**, *21*, 163–168. [CrossRef]
8. Matsumura, O.; Sakuma, Y. Retained Austenite in O.4C-Si-1.2Mn Steel Sheet Intercritically Heated and Austempered. *ISIJ Int.* **1992**, *32*, 4–10. [CrossRef]
9. Xiong, X.C.; Chen, B.; Huang, M.X.; Wang, J.F.; Wang, L. The effect of morphology on the stability of retained austenite in a quenched and partitioned steel. *Scr. Mater.* **2013**, *68*, 321–324. [CrossRef]
10. Timokhina, I.B.; Hodgson, P.D.; Pereloma, E.V. Effect of microstructure on the stability of retained austenite in {TRIP} steels. *Metall. Mater. Trans. A* **2004**, *35*, 2331–2340. [CrossRef]
11. Pereloma, E.V.; Gazder, A.A.; Timokhina, I.B. Addressing retained austenite stability in advanced high strength steels. *Mater. Sci. Forum* **2013**, *738–739*, 212–216. [CrossRef]
12. Blondé, R.; Jimenez-Melero, E.; Zhao, L.; Wright, J.P.; Brück, E.; Van Der Zwaag, S.; Van Dijk, N.H. High-energy X-ray diffraction study on the temperature-dependent mechanical stability of retained austenite in low-alloyed TRIP steels. *Acta Mater.* **2012**, *60*, 565–577. [CrossRef]
13. Yi, J.J.; Kim, I.S.; Choi, H.S. Austenitization during intercritical annealing of an Fe-C-Si-Mn dual-phase steel. *Metall. Trans. A* **1985**, *16*, 1237–1245. [CrossRef]
14. Kang, S.; De Moor, E.; Speer, J.G. Retained Austenite Stabilization Through Solute Partitioning During Intercritical Annealing in C-, Mn-, Al-, Si-, and Cr-Alloyed Steels. *Metall. Mater. Trans. A Phys. Metall. Mater. Sci.* **2015**, *46*, 1005–1011. [CrossRef]
15. Samajdar, I.; Girault, E.; Verlinden, B.; Aernoudt, E.; Van Humbeeck, J. Transformations during intercritical annealing of a TRIP-assisted steel. *ISIJ Int.* **1998**, *38*, 998–1006. [CrossRef]
16. Erişir, E.; Bilir, O.G. Effect of Intercritical Annealing Temperature on Martensite and Bainite Start Temperatures After Partial Austenitization. *Jom* **2016**, *68*, 203–209. [CrossRef]
17. Faral, O. Influence of Continuous Annealing Conditions on Dual-Phase and TRIP Steels for Automotive Application. In Proceedings of the 41st Mechanical Working and Steel Processing Conference, Baltimore, MD, USA, 24–27 October 1999; pp. 253–264.
18. Emadoddin, E.; Akbarzadeh, A.; Daneshi, G. Effect of intercritical annealing on retained austenite characterization in textured TRIP-assisted steel sheet. *Mater. Charact.* **2006**, *57*, 408–413. [CrossRef]
19. Di Schino, A.; Di Nunzio, P.E. Metallurgical aspects related to contact fatigue phenomena in steels for back-up rolls. *Acta Metall. Slovaca* **2017**, *23*, 62–71. [CrossRef]
20. Di Schino, A.; di Nunzio, P.E.; Lopez Turconi, G. Microstructure Evolution during Tempering of Martensite in a Medium-C Steel. *Mater. Sci. Forum* **2007**, *558–559*, 1435–1441. [CrossRef]
21. De Oliveira, P.G.B.; Mariani, F.E.; Casteletti, L.C.; Itman Filho, A.; Neto, A.L.; Totten, G.E. Boro-Austempering Treatment of High-Strength Bainitic Steels. *J. Mater. Eng. Perform.* **2020**, *29*, 3486–3493. [CrossRef]
22. Pashangeh, S.; Somani, M.; Banadkouki, S.S.G. Microstructural evolution in a high-silicon medium carbon steel following quenching and isothermal holding above and below the Ms temperature. *J. Mater. Res. Technol.* **2020**, *9*, 3438–3446.
23. Di Schino, A.; Gaggiotti, M.; Testani, C. Heat Treatment Effect on Microstructure Evolution in a 7% Cr Steel for Forging. *Metals* **2020**, *10*, 808. [CrossRef]

24. Han, J.; Lee, S.J.; Jung, J.G.; Lee, Y.K. The effects of the initial martensite microstructure on the microstructure and tensile properties of intercritically annealed Fe-9Mn-0.05C steel. *Acta Mater.* **2014**, *78*, 369–377. [CrossRef]
25. Kim, S.I.; Jin, Y.H.; Kwak, J.N. Influence of Cooling Process after Hot Rolling on Mechanical Properties of Cold Rolled TRIP Steel. In Proceedings of the Materials Science & Technology 2008 Conference and Exhibition (MS&T Partner Societies), Pittsburgh, PA, USA, 5–9 October 2008; pp. 1784–1802.
26. Pezzato, L.; Gennari, C.; Chukin, D.; Toldo, M.; Sella, F.; Toniolo, M.; Zambon, A.; Brunelli, K.; Dabalà, M. Study of the effect of multiple tempering on the impact toughness of forged s690 structural steel. *Metals* **2020**, *10*, 507. [CrossRef]
27. Spezzapria, M.; Settimi, A.G.; Pezzato, L.; Novella, M.F.; Forzan, M.; Dughiero, F.; Bruschi, S.; Ghiotti, A.; Brunelli, K.; Dabalà, M. Effect of Prior Microstructure and Heating Rate on the Austenitization Kinetics of 39NiCrMo3 Steel. *Steel Res. Int.* **2017**, *88*, 1600267. [CrossRef]
28. Gündüz, S.; Çapar, A. Influence of forging and cooling rate on microstructure and properties of medium carbon microalloy forging steel. *J. Mater. Sci.* **2006**, *41*, 561–564. [CrossRef]
29. Babu, S.S.; Bhadeshia, H.K.D.H. A direct study of grain boundary allotriomorphic ferrite crystallography. *Mater. Sci. Eng. A* **1991**, *142*, 209–219. [CrossRef]
30. Xu, P.; Bai, B.; Yin, F.; Fang, H.; Nagai, K. Microstructure control and wear resistance of grain boundary allotriomorphic ferrite/granular bainite duplex steel. *Mater. Sci. Eng. A* **2004**, *385*, 65–73. [CrossRef]
31. Ahmad, E.; Manzoor, T.; Ziai, M.M.A.; Hussain, N. Effect of martensite morphology on tensile deformation of dual-phase steel. *J. Mater. Eng. Perform.* **2012**, *21*, 382–387. [CrossRef]
32. Luo, Q. A new XRD method to quantify plate and lath martensites of hardened medium-carbon steel. *J. Mater. Eng. Perform.* **2016**, *25*, 2170–2179. [CrossRef]
33. Mirnik, M.; Strohal, P.; Wrischer, M.; TeŽak, B. Elektronenmikroskopische Untersuchung der Silberjodidfällung. *Kolloid Z.* **1958**, *160*, 146–156. [CrossRef]
34. Yescas, M.A.; Bhadeshia, H.K.D.H. Model for the maximum fraction of retained austenite in austempered ductile cast iron. *Mater. Sci. Eng. A* **2002**, *333*, 60–66. [CrossRef]
35. Podder, A.S.; Bhadeshia, H.K.D.H. Thermal Stability of Austenite Retained in Bainitic Steels. *Mater. Sci. Eng. A* **2010**, *527*, 2121–2128. [CrossRef]
36. Sherif, M.Y.; Mateo, C.G.; Sourmail, T.; Bhadeshia, H.K.D.H. Stability of retained austenite in TRIP-assisted steels. *Mater. Sci. Technol.* **2004**, *20*, 319–322. [CrossRef]
37. Ryu, J.H.; Kim, D.I.; Kim, H.S.; Bhadeshia, H.K.D.H.; Suh, D.W. Strain partitioning and mechanical stability of retained austenite. *Scr. Mater.* **2010**, *63*, 297–299. [CrossRef]
38. Sugimoto, K.I.; Yu, B.; Mukai, Y.I.; Ikeda, S. Microstructure and formability of aluminum bearing TRIP-aided steels with annealed martensite matrix. *ISIJ Int.* **2005**, *45*, 1194–1200. [CrossRef]
39. Reisner, G.; Werner, E.A.; Fischer, F.D. Micromechanical modeling of martensitic transformation in random microstructures. *Int. J. Solids Struct.* **1998**, *35*, 2457–2473. [CrossRef]
40. Carter, C.B.; Williams, D.B. *Transmission Electron Microscopy*; Springer: Boston, MA, USA, 1996.
41. Qian, L.; Zhou, Q.; Zhang, F.; Meng, J.; Zhang, M.; Tian, Y. Microstructure and mechanical properties of a low carbon carbide-free bainitic steel co-alloyed with Al and Si. *Mater. Des.* **2012**, *39*, 264–268. [CrossRef]
42. Toribio, J.; González, B.; Matos, J.C.; Ayaso, F.J. Influence of microstructure on strength and ductility in fully pearlitic steels. *Metals* **2016**, *6*, 318. [CrossRef]
43. Shi, W.; Li, L.; Yang, C.X.; Fu, R.; Wang, L.; Wollants, P. Strain-induced transformation of retained austenite in low-carbon low-silicon TRIP steel containing aluminum and vanadium. *Mater. Sci. Eng. A* **2006**, *429*, 247–251. [CrossRef]
44. Bhadeshia, H.K.D.H.; Edmonds, D.V. The Distribution of Retained Austenite in MArtensite and the Influence of Inter-lath Crystallography. In Proceedings of the International Conference on Martensitic Transformations, Cambridge, MA, USA, 24–29 June 1979; pp. 28–33.

45. Lee, Y.K. Empirical formula of isothermal bainite start temperature of steels. *J. Mater. Sci. Lett.* **2002**, *21*, 1253–1255. [CrossRef]
46. Krauss, G. *Steels: Processing, Structure, and Performance*; ASM International: : New York, NY, USA, 2005; ISBN 0871708175.